NAG5 - 7942

TP/IN/43

Resolution Enhancement of Spaceborne Radiometer Images

Hamid Krim
ECE Dept.
NCSU, Raleigh NC

Our progress over the last year has been along several dimensions.
   a. Exploration and understanding of Earth Observatory System (EOS) mission with available data from NASA
   b. Comprehensive review of state of the art techniques and uncovering of limitations to be investigated (e.g. computational, algorithmic ...)
   c. Preliminary development of resolution enhancement algorithms

1) Background

• Radiometry

With the advent of well-collaborated satellite microwave radiometers, it is now possible to obtain long time series of geophysical parameters that are important for studying the global hydrologic cycle and earth radiation budget.

Over the world's ocean, these radiometers simultaneously measure profiles of air temperature and the three phases of atmospheric water (vapor, liquid, and ice). In addition, surface parameters such as the near surface wind speed, the sea surface temperature, and the sea ice type and concentration can be retrieved.

The special sensor microwaves imager SSM/I has wide application in atmospheric remote sensing over the ocean and provide essential inputs to numerical weather-prediction models. SSM/I data has also been used for land and ice studies, including snow cover classification measurements of soil and plant moisture contents, atmospheric moisture over land, land surface temperature and mapping polar ice.

The brightness temperature observed by SSM/I is function of the effective brightness temperature of the earth's surface and the emission scattering and attenuation of the atmosphere. Advanced Microwave Scanning Radiometer (AMSR) is a new instrument that will measure the earth radiation over the spectral range from 7 to 90 GHz. Over the world's ocean, it will be possible to retrieve the four important geographical parameters SST, wind speed, vertically integrated water vapor, vertically integrated cloud liquid water L.

• Resolution Enhancement

Due to the diffraction of differences in antenna pointing directions, microwave radiometer antenna gain patterns of different frequency may differ in size or location on the earth surface while physical inversion algorithms may assume that observations describe consistent locations. Therefore, the mismatch in the resolution becomes a critical problem when observations at many different frequencies must be combined to retrieve single parameters, which requires that the area on the surface imaged by different channels be the same.

The obvious solution to this problem is to average the high-resolution measurements to match the lower resolution data. However, this solution is not recommended due to the non-linearity in the physical model that relates the measured brightness temperature to the geophysical parameters. A much more desirable solution, is to enhance the low-resolution

data to match the higher resolution data. The theory is based on the fact that the density of the measurements made by the space borne radiometer is higher than the resolution of the instrument, which means that it is possible to take advantage of over sampling to reconstruct a higher resolution image from low-resolution data.

2) Survey of Image Restoration Techniques

The purpose of image restoration is usually formulated as the estimation of an improved image S of the original image S when a noisy blurred version Z given by:

$$Z = HS + V \qquad (1)$$

is observed, where the blurring matrix H is known and some statistical knowledge about V and S is assumed to be available. Specifically, we will assume that the image model $S = AS + W$ is feasible. The direct inversion of the matrix H does not lead to useful restoration because of the ill conditionedness of H.

Procedures to stabilize the inversion of an ill conditioned matrix are called regularization methods and make nearly always use of a priori knowledge about the original image and the noise.

The main objective in solving ill posed problems is the construction of physically acceptable and meaningful approximation of the true solution that is sufficiently stable from a computational point of view. If we are to obtain a useful approximate solution to (1), we must modify the problem in such a way that the solution becomes less sensitive to noise in the observed image (well posed problem). At the same time the solution of the modified problem must be close to the solution of the original problem. The process of achieving a compromise between these conflicting goals is referred to as regularization and is typically controlled by one or more regularization parameter. Nearly, all concepts used in regularization are based on incorporating a priori knowledge about either the true solution or the noise into the algorithm which solves the image restoration problem

2-1) Tikhonov-Miller Regularization:

The idea is to define a criterion to select an approximate solution from a set of feasible solutions. On the basis of the observed model (1) it is plausible that the class of feasible solutions is described by :

$$\Phi(S) = \|Z - HS\| \le \|V\| = \varepsilon \qquad (2)$$

The bound ε is related to uncertainty or noise in the observed image Z and can usually be estimated from smooth image region. Tikhonov defined the regularized solution as the' one which minimizes the stabilizing functional $\Omega(S)$ in the set of feasible solutions. Although a wide class of different stabilizing functionals is available, including for example the max

3

power and max entropy measures, usually a stabilizing functional of the following form chosen to facilitate the mathematical analysis of the problem

$$\Omega(S) = \|CS\| \qquad (3)$$

Here C is a real valued matrix of size $M \times N$ known as the regularizing operator. The computation of the regularized solution now reduces to the minimization of (2) subject to (3). Using the method of undetermined Lagrange multiplier we need to minimize the objective function:

$$\Phi(S) = \|Z - HS\|^2 + \alpha \|CS\|^2 \qquad (4)$$

with respect to S. The regularization parameter α is chosen so that (2) is satisfied with equality. [1] proposed a empirical criterion based on CRESO (composite residual and smoothing operator) for finding the optimum value of α^{opt} which gives the solution S closest to its initial value. According to this criterion α^{opt} is the value α that gives the first local maximum of the function:

$$C(\alpha) = \|S\|^2 + 2\alpha \frac{d}{d\alpha} \|S\|^2 \qquad (5)$$

Among the solutions satisfying a reasonable choice is the one which minimizes $\Phi(S)$ called the Tikhonov Miller regularized solution. This minimization is straight forward and leads to the following solution:

$$(H'H + \alpha C'C)^{-1} S = H'Z \qquad (6)$$

provided that $(H'H + \alpha C'C)^{-1}$ is invertible.

Iterative Solutions

Iterative solutions offer the advantage that no matrix inverses need to be implemented and that additional deterministic constraints can be incorporated into the solution algorithms. To derive the iterative Tikhonov Miller regularized restoration algorithm, many methods were proposed [2].

- **Steepest Descent Method:**

The steepest descent method is used to minimize the objective function $\Phi(S)$ by using the following iteration:

$$S^{k+1} = S^k + \beta r^k$$
$$= S^k - \frac{1}{2} \beta \nabla_S \Phi(S)|_{S_k}$$
$$= S^k - \beta((H'H + \alpha C'C)S^k - HZ)$$

$$= (I - \alpha\beta C'C)S^k + \beta H'(Z - HS^k) \dots\dots\dots\dots\dots\dots\dots\dots\dots\dots\dots\dots\dots\dots\dots\dots(7)$$

This iteration reduces the to Van Cittert iteration if $\alpha = 0$ which is the case of no regularization.

$$S^{k+1} = S^k + \beta H'(Z - HS^k) \qquad (8)$$

The term $(I - \alpha\beta C'C)$ in () behaves like a low pass filter suppressing the noise in the iterates. The characteristics of this term are obviously related to the properties of the original image because the regularizing operator C is closely related to the image model A.

Analysis of Convergence Speed

The convergence speed of an iterative algorithm towards its limiting solution can be quantified by its convergence rate. An iterative scheme converges geometrically with order R if the error $\left\| S^k - S^\infty \right\|$ for k sufficiently large can be given as

$$\left\| S^k - S^\infty \right\| \cong K \left\| S^k - S^\infty \right\|^R, R \geq 1 \qquad (9)$$

A large value of K corresponds to a slow convergence while a small value indicates fast convergence. Further, the larger the convergence order is, the faster the algorithm converges. For R=1, the process is said to converge linearly in which case (9) is conveniently written as:

$$\left\| S^k - S^\infty \right\| \leq K^k \left\| S^0 - S^\infty \right\|^R \qquad (10)$$

and $0 \leq K \leq 1$. For K=0, the convergence is said to be superlinear or in other words the iterative process terminates within a finite number of iterations. While for K=1, the convergence is sublinear.

Iterative schemes which minimizes a quadratic objective function $\Phi(S)$ by the method of steepest descent can all be regarded as members of the following generic iterations

$$S^{k+1} = S^k + \beta((h - BS_k) \qquad (11)$$

for nonsingular matrix B, we have $S^\infty = B^{-1}H$. The following relation can then be established:

$$S^{k+1} - S^\infty = (I - \beta B)S^k + \beta h - S^\infty$$
$$= (I - \beta B)S^k + \beta BS^\infty - S^\infty$$
$$= (I - \beta B)(S^k - S^\infty) \qquad (12)$$

5

$$\left\| S^k - S^\infty \right\| \le \left\| I - \beta B \right\| \left\| S^k - S^\infty \right\|^R \qquad (13)$$

Here $\left\| I - \beta B \right\|$ denotes the norm of the matrix which is given by its largest eigen value. Thus, if we let ρ_{min} be the eigen value of B with smallest norm then (13) becomes :

$$\left\| S^k - S^\infty \right\| \le \left| 1 - \beta \rho_{min} \right| \left\| S^k - S^\infty \right\|^R \qquad (14)$$

Hence, iterative schemes of the type (12) converges linearly with a convergence rate of $\left| 1 - \beta \rho_{min} \right|$. For the iteration (12) , we have $(I - \beta B) = I - \beta (H'H + \alpha C'C)$ and ρ_{min} is the smallest eigen value of $(H'H + \alpha C'C)$.

Since the smallest eigen value is nearly always close to zero in an image restoration application, the iteration (12) converges slowly.

In general, the convergence rate depends on the regularization parameter α because ρ_{min} is a function of α. If α is increased, i.e. if the restoration problem is regularized more strongly, ρ_{min} attains a larger value by which the speed of convergence increases as well. Also, β was assumed to have fixed value satisfying the condition:

$$0 < \beta < \frac{2}{\left| \rho_{max} \right|} \qquad (15)$$

where ρ_{max} is the largest eigenvalue of the matrix $(H'H + \alpha C'C)$.

But since β controls the convergence rate as follows from (), it is desirable to optimize its value at each iteration step.

- ### Conjugate Gradient Method

Motivated by the desire to achieve more rapid convergence, the method of conjugate gradient has been successfully used in optimization theory. Conjugate direction methods which were originally introduced for purely quadratic problems, can be viewed as special orthogonal expansion of the solution of the minimization problem. This expansion is generated by making use of information from previous iteration steps. One advantage of this method is its convergence in a finite number of iterations steps when exact arithmetic is used (no rounding errors) the convergence is superlinear. When nonexact arithmetic is used or the problem is non quadratic, the method will no longer converge in a finite number of iterations because the conjugacy condition will no longer holds.

It has been experimentally shown, however, that the conjugate gradient method converges always faster than the method of steepest descent, while the computational complexity is not significantly increased. The basic form of the conjugate gradient algorithm which thus represents an alternative to the iteration (12) is given by:

$$r^k = -\frac{1}{2}\nabla_S \Phi(S)\big|_{S_k} = -(H'H + \alpha C'C)S^k + H'Z$$

$$p_k = r_k + \gamma_k p_k$$
$$S^{k+1} = S^k + \beta_k p_k \qquad\qquad (16)$$

In this scheme, S^k is modified in the direction of the vector p^k instead of the steepest descent direction r^k. The parameter γ^k controls the conjugacy of the subsequent direction p^k. For $\gamma^k \to 0$, the iterations reduce to (7). It can be shown that the values γ^k and β^k are given by:

$$\gamma_k = \frac{\|r_k\|^2}{\|r_{k-1}\|^2} \qquad\qquad (17)$$

$$\beta^k = \frac{r_k' p_k}{\|Hp_k\|^2 + \alpha\|Cp_k\|^2} \qquad\qquad (18)$$

The conjugate gradient method converges linearly with a convergence rate given by:

$$\|S^k - S^\infty\| \le K\left(\frac{\sqrt{|\rho_{max}|} - \sqrt{|\rho_{min}|}}{\sqrt{|\rho_{max}|} + \sqrt{|\rho_{min}|}}\right)^k \qquad\qquad (19)$$

Although (19) is rather upper bound to the convergence rate of the conjugate gradients iterations (for example, it does not show that the method of conjugate gradient converges within a finite number of iterations, it is still has a higher convergence speed than the method of steepest descent. In addition to this, experimental results exhibit a convergence speed much larger than indicated by the bound (15).

Observe that the difference in computational complexity between the method of steepest descent and the conjugate gradients algorithm merely consists of the computations of p^k and γ^k which is insignificant compared with the other computations required within a single iteration step.

- **Preconditioned Conjugate Gradient Methods**

The convergence rate of iterative methods depends on the spectrum of matrix H. Generally speaking, the method converges faster if H has smaller condition number or clustered eigen values. In order to accelerate the convergence rate we may consider the solution of a new equivalent system of equations:

$$P^{-1}Z = P^{-1}HS \qquad\qquad (20)$$

instead of the original one where P can be easily interpreted and $P^{-1}H$ has better spectral property than H. the matrix P is usually called the preconditioner of the matrix H. To impalement preconditioning, the matrix vector product $P^{-1}v$ for a certain vector v is performed at each iteration. Various preconditioning techniques have been introduced in solving elliptic partial differential equations and Toeplitz systems of equations.

Preconditioned CGN method was introduced in [4], where the conjugate gradient methods is applied to the normal equations $H'Z = H'HS$ when the matrix H is not symmetric positive definite since $H'H$ is symmetric.
Consider the model:

$$Y = AS \qquad (21)$$

Where A is a block Toeplitz matrix (symmetric positive semi definite). A good preconditioner for A is a matrix P that approximates A well in the sense that the spectrum of the preconditioned matrix $P^{-1}A$
is clustered around 1 or has small condition number and that can be inverted efficiently.
One preconditioning technique has been generalized from point to block Toeplitz matrices by Ku and Kuo [3]. They proposed to use a block circulant matrix as a preconditioner for the block Toeplitz matrix since the block circulant matrix can be easily inverted via 2-D FFT.
Let A be a block Toeplitz matrix containing $N{\times}N$ blocks with $M{\times}M$ elements per block:

$$A = \begin{bmatrix} A_0 & A_{-1} & & A_{2-N} & A_{1-N} \\ A_1 & & & & \\ & & & & \\ A_{N-1} & A_{N-2} & & & A_0 \end{bmatrix} \qquad (22)$$

Where A_n with $|n| < N - 1$ are $M{\times}M$ Toeplitz matrices with elements $[A_n] = a_{i-j,n}$, $1 \le i, j \le M$
We use the following $MN{\times}MN$ block circulant matrix as its preconditioner

$$P = \begin{bmatrix} P_0 & P_{N-1} & & P_1 \\ & & & \\ & & & \\ P_{N-1} & A_{N-2} & & P_0 \end{bmatrix} \qquad (23)$$

Where

$$P_n = \begin{cases} \widetilde{P}_n, & n = 0 \\ \widetilde{P}_n + \widetilde{P}_{N-n}, & 1 < n < N - n \end{cases}$$

8

and where $\widetilde{P}_n$ is circulant matrix with $a_{0,n}, a_{-1,n} + a_{M-1,n}, a_{-2,n} + a_{M-2,n}, \ldots a_{1-M,n} + a_{1-M,n} + a_{1,n}$ as the first row.

From the construction, we see that P is an approximation of A and the matrix vector product $P^{-1}v$ for any v can be computed via 2-D FFT.

The PCGN method is summarized as follows:

Arbitrary x_0, $r_0 = y - Ax_0$, $p_0 = 0$, $\beta_0 = 0$

Iteration $k=1,2,\ldots$

$$z_{k-1} = M^{-1}A^t r_{k-1}$$

$$p_k = Z_{k-1} + \beta_k p_{k-1}$$

$$\alpha_k = \frac{(z_{k-1}, A^t r_{k-1})}{\|Ap_k\|^2}$$

$$x_k = x_{k-1} + \alpha_k p_k$$

$$r_k = r_{k-1} - \alpha_k A p_k$$

$$\alpha_k = \frac{(z_k, A^t r_k)}{(z_{k-1}, A^t r_{k-1})} \qquad (24)$$

where M is the preconditioner. $M = P^t P$.

The convergence rate of the preconditioned iterative method depends on the eigen value distribution of the preconditioned matrix $(P^t P)^{-1}$.

The preconditioned iterative methods converge faster if $(P^t P)^{-1} A^t A$ has clustered eigen values and /or small condition number.

Kuo [3] studied the eigenvalues distribution of the matrices $A^t A$ and $(P^t P)^{-1} A^t A$ with different values of the image size where they showed that the eigen values of the preconditioned matrices have much better clustering property that the original ones.

2-2) Algebraic reconstruction techniques ART

ART is a reconstruction technique that was recognized to be identical to the algorithms of solving the system of liner equations $Z=HS$ where Z,H,S are as defined in (1).

ART are based on an iterative process, which starts from an initial approximation S0 to the image vector. In an iterative step, the current iterate S^k is refined (or corrected) to a new iterate S^{k+1} by taking into account only a single measurement, say the ith measurement and changing only the image values of the pixels which intersect this measurement. The discrepancy between the measurement Z_i and the pseudo projection data $\sum_{j=1}^{N} h_{ij} S_j^k$ obtained

9

from the current image S^k is redistributed among the pixels along the ith measurement proportionally to their weights h_{ij} in the whole measurement.

In this way, the pixel values covered by the ith measurement are corrected to conform with the ith measurement without changing the rest of the image. Denoting $h^i = (h_{ij})_{j=1}^n$ as a vector in R^n. The following algorithm describes this process:

$S^0 \in R^N$

Typical step

$$S^{k+1} = S^k + \frac{Z_i - <h^i, S^k>}{\|h^i\|^2} h^i \qquad (25)$$

Where: $<u,v> = \sum_{j=1}^n u_j v_j$ and $\|u\|^2 = <u,u>$.

and the measurements are chosen cyclically: $i = i_k = k(\mathrm{mod}\,M) + 1$.

Censor [5] investigate the convergence behavior of ART when applied to ill posed and inconsistent systems of equations and proposed to use relaxation parameters which are a sequence $(\lambda_k)_{k=0}^\infty$ of real numbers usually confined to an interval

$\varepsilon_1 \leq \lambda_k \leq 2 - \varepsilon_2$, $\varepsilon_1, \varepsilon_2 > 0$

Which appear in the typical step of ART as:

$$S^{k+1} = S^k + \lambda_k \frac{Z_i - <h^i, S^k>}{\|h^i\|^2} h^i \qquad (26)$$

The relaxation parameters allow are to overdo or undo the orthogonal projection prescribed by ART.

2-3)   Block ART

Block ART were first introduced by Eggermont et-al [] to solve the system of ill posed linear equations $Z=HS$, where the MxN matrix H may be partitioned in two ways as:

$$H = \begin{bmatrix} h_1^t \\ h_2^t \\ \\ \\ h_{LK}^t \end{bmatrix} = \begin{bmatrix} H_1 \\ H_2 \\ \\ \\ H_M \end{bmatrix}$$

here h_i is an N dimensional vector and its transpose h_i^t constitutes the ith row of H. each matrix H_i is an LxN block of rows of H and assuming there are K blocks of width L obviously means that $M=LK$.

The M dimensional vector Z is partitioned as

$$Z^t = (Z_1, Z_2, \ldots, Z_{LK}) = (z_1^t, z_2^t, \ldots, z_K^t)$$

where z_i is a block of length L of elements of Z.

The block ART is the following group of iterative variations
Initialization
$S^0 \in R^N$ is arbitrary
Typical step:

$$S^{k+1} = S^k + H_i^* \Omega^k (Z_i - H_i S^k) \tag{27}$$

where Ω^k is an LxL matrix called relaxation matrix, H_i^* is the Moore-Penrose inverse of H_i and the blocks with respect to which the iteration is performed are chosen in a cyclic manner: $i = i_k = k(\mod M) + 1$, $k=1,2,\ldots$

The case $\Omega^k = \lambda_k I$ with I standing for an LxL identity matrix coincides with ART algorithm when $L=1$.

In addition, Long et-al, showed that block AART is equivalent to a least squares estimate in the limit of infinite iterations based on the minimization problem:

Minimize $\|S\|^2$ *subject to Z=HS.*

Which is equivalent to Tikhonov regularized solution.

2-4) Entropy Regularization (MART)

The use of entropy is rigorously founded in several areas. In image reconstruction from projections several authors advocate the maximum entropy approach. From the standpoint of information theory, this approach is conceptually attractive. It yields the image with the lowest information content consistent with the available data.

Thus with this approach one avoids introducing extraneous information or artificial structure. The problem of reconstructing a source from a finite number of views is known to be indeterminate. A maximum entropy method thus seems attractive for this problem especially when the available projection data are incomplete or degraded by noise errors.

By Frieden's model [6], the most likely object scene implied by given image data is found to obey a principle of maximum entropy.

Entropy optimization refers to the problem of maximizing the functional

$$f(S) = -\sum_{j=1}^{n} S_j \ln S_j \quad \text{over the constraint } Z=HS.$$

A typical problem would be

Maximize: $-\sum_{j=1}^{n} S_j \ln S_j$ subject to $Z=HS$ (28)

and $S \geq 0$

A variety of iterative algorithms are available to solve () but no practical direct form solutions are known.

Lent [5] suggested the following algorithm and proved that it actually converges under some reasonable conditions to the solution of the maximum entropy problem.

$$S_j^{k+1} = S^k \left(\frac{Z_i}{< h^i, S^k >} \right)^{\lambda_k h_{ij}} \tag{28}$$

where λ_k is a relaxation parameter.

Equations are taken cyclically, i.e. $i = i_k = k(\bmod M) + 1$.

2-5) Variational Methods

In the previous sections we showed that the classic setting for solving the image reconstruction inverse problem is the least squares minimization. However, regularization is needed when solving the ill posed problems to neutralize some of the ill conditioning but it also removes sharp edges and similar distinguishable features. Hence, the choice of the regularizing function is an issue.

In variational approach, an image is defined as a real function S: $S : \Omega \to R$, where Ω is an open bounded subset of R^2.

The formulation of the image reconstruction using variational methods is based on solving the optimization problem

Minimize $\Phi(S)$ subject to $Z=HS$

i.e.

$$\hat{S} = \arg\min_S \left\{ \Phi(S) + \frac{\lambda}{2} \|Z - HS\|^2 \right\} \tag{29}$$

The critical issue is the choice of the variational integral. One of the widely used variational integrals based on geometrical argument is the total variation proposed by Ruden et-al and defined as follows

$$TV(S) = \int_{\Omega} |\nabla S| d\omega \tag{30}$$

the total variation method basically consists of finding an estimate $\hat{S}$ for the original image S with the smallest total variation among all the images satisfying the noise constraint $\|Z - HS\| = \sigma^2$ where σ^2 is assumed known. Roughly TV permits image intensity to have sharp jumps, but it limits spurious oscillations. Regularized least squares, on the other hand, tends to smooth out sharp jumps because it controls the second derivative of the image intensity.

An iterative solution for the optimization problem can be obtained using gradient descent method as follows:

$$S^{k+1} = S^k + \alpha\left[\nabla(\nabla S^k) - \lambda(Z - HS^k)\right] \qquad (31)$$

Ben Hamza and Krim [7] introduced an entropic variational approach based on the concept of negentropy variational integral which is defined as:

$$H(S) = \int_\Omega H(|\nabla S|)d\omega = \int_\Omega |\nabla S|\log|\nabla S|d\omega \qquad (32)$$

Then the minimization problem can be written as:

$$\hat{S} = \arg\min_S\left\{\int_\Omega |\nabla S|\log(|\nabla S| + \frac{\lambda}{2}\|Z - HS\|^2 d\omega\right\} \qquad (33)$$

and the iterative solution can be written as:

$$S^{k+1} = S^k + \alpha\left[\nabla(\frac{1 + \log|\nabla S^k|}{|\nabla S^k|}\nabla S^k) - \lambda(Z - HS^k)\right] \qquad (34)$$

3) Spatial Resolution Enhancement of SSM/I Data

The special sensor microwave imager SSM/I, a satellite passive microwave radiometer observes a large portion of the earth's surface and measures the top atmosphere brightness temperature at 19.35,37,85 GHz in both the horizontal and the vertical polarizations and at 22.235 GHz channel in the vertical polarization only.

The instrument flies at an altitude of 833km and scans the earth in a conical scan 1400km wide. The SSM/I samples data in seven channels covering four microwave frequencies – table (1). The lower frequencies of the instrument (19,22,37) are sampled every 25km along the scan and every 25km along the track, while the other high frequency is sampled 12.5km.

Due to the physical limitations on the SSM/I antenna size the data have relatively poor spatial resolution. The spatial resolution of a passive microwave sensor depends both on the antenna size and frequency. Because the SSM/I instrument uses on parabolic reflector for all four frequencies, the spatial resolution improves with increasing frequency.

To retrieve geophysical parameters from SSM/I measurements take at different frequencies requires that the area on the surface imaged by different channels be the same in order to obtain more accurate measurements of geophysical parameters, it would be preferable to improve the resolution of data at low frequencies to that of higher

13

frequencies. Table(1) shows the SSM/I channels and the corresponding sizes of foot prints and sampling intervals. Correction techniques for matching the resolution of all frequencies of the SSM/I to the 25 km spatial resolution of the 37 GHz were presented in [8]-[13].

Table 1

Channel Frequency	Polarization	Resolution (km) along		Sampling interval (km) Along track/scan
		Track	Scan	
19.35	V/H	69	43	25
22.235	V	60	40	25
37	V/H	37	28	25
85.5	V/H	15	13	12.5

Backus & Gilbert first proposed the methodology for the correction techniques. In essence, the theory contends that if the density of the measurements made by the satellite is higher than the resolution of the instrument, then it is possible to find a linear combination of surrounding measurements that yields results at a higher spatial resolution than the original data. The tradeoff of r higher spatial resolution in this procedure is the rapid amplification of instrument noise. Other techniques based on algebraic reconstruction techniques provide an estimate of the brightness temperature of each element of a rectilinear grid of pixels. The problem reduces to the solution of a system of linear equations that is ill conditioned by using iterative algorithms. ART requires less computations than BGI methods, but on the other hand, BGI methods provide a tradeoff between noise and resolution enhancement.

3-1) BGI Algorithm

An SSM/I measurement can be modeled as a product of the surface brightness temperature and the antenna pattern. The ith measurement $T_A(i)$ is obtained by integrating the product of the surface brightness $T_B(x,y)$ and the antenna at the surface $G_i(x,y)$

$$T_A(i) = \overline{G}_i^{-1} \iint G_i(x,y)T_b(x,y)dxdy \qquad (35)$$

$$\overline{G}_i^{-1} = \iint G_i(x,y)dxdy \qquad (36)$$

14

Where integrals over surface area are corresponding to he non-negligible gain of the antenna. The dependence of G on I arises from bore sight pointing of the antenna, which changes as the antenna scans the surface.

The antenna pattern acts as a low pass filter of the surface brightness limiting the effective resolution of the measurements. The BGI algorithm is an inversion method for solving the integrals equations. The algorithm is used to determine surface brightness from integrated over lapping antenna patterns. When employed for spatial resolution enhancement, the BGI method produces a weighted least squares estimate of the surface brightness temperature on a rectilinear surface grid finer than the intrinsic resolution of the sensor. Given a set of antenna temperature measurements $T_A(i)$ with associated antenna gain patterns $G_i(x, y)$, the algorithm estimates the brightness temperature $T_B(x_j, y_j)$ for each pixel (x_j, y_j) of the enhanced resolution image.

To estimate Tb for a given pixel, the BGI method uses linear combination of N nearby measurements

$$T_B(x_j, y_j) = \sum_{i=1}^{M} a_{ij} T_A(i) \tag{37}$$

coefficients a_{ij} are determined from measurement geometry and the noise correlation matrix. These coefficients are different for every pixel due to the varying antenna geometry over the swath.
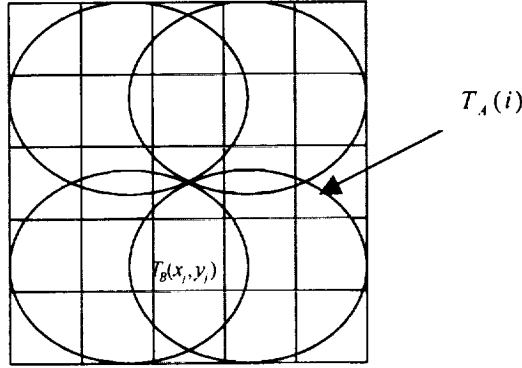

Figure 1: Reconstructing high-resolution brightness temperature from $T_A(i)$ measurements.

Substituting (1) into (3)

$$T_B(x_j, y_j) = \sum_{i=1}^{M} a_{ij} \iint G_i(x, y) T_B(x, y) = \iint [a_{ij} G(x, y)] T_B(x, y) dx dy \tag{38}$$

15

If one can find coefficients a_{ij} such that the bracketed term becomes the <u>dirac delta</u> function $\delta(x_j - x, y_j - y)$, then (38) would be an exact solution to the problem and (37) could be used to find the actual scene brightness temperature at any desired resolution. In practice, however, the finite number of measurements makes it impossible to find such a set of coefficients a_{ij}.

Instead, we confine ourselves to selecting a set of coefficients a_{ij} which causes the bracketed term to most closely produce some desired behavior. In particular, we look for a set of coefficients a_{ij} which make the bracketed term appear like the gain function $G(x, y)$ of the 37 GHz channel. It must be understood that $T_B(x_j, y_j)$ is no longer the true scene brightness temperature but the brightness temperature as it would be seen at the 37 GHz resolution. By using the actual 37 GHz antenna function as the match function, no correlation is necessary for the 37 GHz s. The 37 GHz antenna function also has a footprint which is most similar in size to the 25km spatial sampling distance if the instrument.

To find the coefficients a_{ij}, consider the quantity:

$$Q_0 = \iint \left[\sum_{i=1}^{M} a_{ij} G_i(x, y) - G^{37}(x, y) \right]^2 dx dy \qquad (39)$$

Where $G^{37}(x, y)$ is the gain function of the 37 GHz channel.

Minimizing Q_0 with respect to a_{ij} subject to the constraint that proper normalization be presented.

$$\iint \sum_{i=1}^{M} a_{ij} G_i(x, y) dx dy = 1 \qquad (40)$$

should produce the best correlation coefficient possible in the least square sense.

The above treatment assumes the antenna measurements to be exact. In practice, however, the antenna temperature $T_A(i)$ will not be known exactly, but rather will contain some random noise whose variance is given by $(\Delta T_{rms})^2$

Thus noisy $T_A(i)$ can be expressed as

$$\hat{T}_A(i) = T_A(i) + \varepsilon_i \qquad (41)$$

Where: $\hat{T}_A(i)$ is the mean value of $T_A(i)$

ε_i: random noise component of zero mean.

The high-resolution brightness temperature can be expressed as:

$$T_{B_i} = a^t \hat{T}_A = a^t T_A + a^t \varepsilon \qquad (42)$$

16

where T_{B_j} is a simplified notation of $T_B(x_j, y_j)$, $a^t = [a_{1j} a_{2j} ... a_{Mj}]$,
$T_A = [T_A(1), T_A(2), ..., T_A(M)]^T$.

And the noise variance of T_{B_j} is:

$$\sigma^2 = E[(\hat{T}_{B_j} - T_{B_j})^2]$$
$$= E[(a\varepsilon)(a\varepsilon)']$$
$$= E[(a\varepsilon\varepsilon'a)]$$
$$= aE[\varepsilon\varepsilon']a$$
$$= a\Im a \tag{43}$$

Where $\Im$ is the noise covariance matrix of instrument noise process appearing in the sampled antenna temperature and is a function of system noise temperature, predetection bandwidth and receiver low pass filter when the noise in each sample is uncorrelated and equal, then e^2 is proportional to the sum of squares of a_{ij} times the variance of instrument noise. That is:

$$\Im = \begin{bmatrix} (\Delta T_{rms})^2 & & & \\ & \cdot & & \\ & & \cdot & \\ & & & (\Delta T_{rms})^2 \end{bmatrix} \tag{44}$$

a diagonal matrix.

Because we not only want to increase the resolution but rather to avoid introducing any drastic increases in the instrument noise. We thus seek a compromise between resolution enhancement and noise.
Rather than Q_0 we minimize:

$$Q = Q_0 \cos\gamma + e^2 w \sin\gamma \tag{45}$$

Where w is a scale factor used to make the two terms on the right hand side of (45) dimensionally and numerically compatible. γ can be varied between 0 and $\frac{\pi}{2}$ to place various degrees of emphasis on either the resolution enhancement or the noise suppression in the estimate of $T_B(x_j, y_j)$.
The coefficients a_{ij}, can now be expressed as:

$$a = S^{-1}[v\cos\gamma - \lambda u] \tag{46}$$

17

where:

$$\lambda = \frac{-1 + uS^{-1}v\cos\gamma}{uS^{-1}u}$$

$$S_{llk} = \cos\gamma \iint G_l G_k \, dxdy + \delta_{ij}(\Delta T_{rms})^2 w\sin\gamma$$

$$u = [u_1, u_2, \dots, u_M]^T,$$

$$v = [v_1, v_2, \dots, v_M]^T$$

$$u_l = \iint G_l \, dxdy, \quad l,k=1,2,\dots,M$$

$$v_l = \iint G^{37} G_l \, dxdy$$

δ_{ij} is kronecker delta function.

Note that these coefficients are different for every pixel due to the varying antenna geometry over the swath.

There are two tuning parameters, the dimensional parameter w and noise parameter γ.

w is arbitrary. Following [11] w is set to 0.001. The noise tuning parameter γ which can vary from 0 to $\frac{\pi}{2}$ controls the tradeoff between the resolution and noise parameter.

γ can be subjectively selected to optimize the resulting image. The optimum value for γ is dependent on the value of ΔT used for the noise level.

In general γ is different for each SSM/I channel. [12] developed an objective function technique for selecting γ for the 19, 22 and 37 GHz channels based on maximizing the correlation between the 85 GHz channels and the particular channel of interest.

Note that when multiple images with exactly the same measurements and pixel locations are processed, the BGI enhancement coefficients may be stored and reused.

The BGI produced image is affected by the definition of nearby N measurements and the relative location and gain patterns of the measurements included in the sum (37). Restricting the size of the local region defining nearby measurements reduces the computational load at the expense of accuracy. Increasing the size of the local are (and M) to include additional measurements can improve the accuracy of the resolution enhancement but may significantly increase the computational load.

Previous investigators have used a fixed range of angles around the antenna pointing direction to define nearby measurements. This approach can lead to numerical problems in the matrix inversion step of the algorithm if the angle range is large enough to include directions with very small region.

Long [14], defined nearby measurements as those measurements that have nonnegligible gain at the pixel of interest. A threshold is used to determine if the gain is nonnegligible. The measurement is used in (37) only if the relative antenna gain at the pixel of interest is greater than the threshold. Setting a lower gain threshold results in more measurements being used in () but increases the noise level of the images.

18

The exact number of nearby measurements used at a given pixel is a function of the gain pattern and sampling geometry and varies across the swath and for each channel.

The BGI approach produces adequate enhancement of the spatial resolution to make such a correction worthwhile.

Results obtained in [14] suggests that the BGI technique decreases brightness temperature differences by over 50% for the low resolution channels with only a modest increase in random noise.

The correction can also help to better resolve small features which would otherwise be lost due to the lack of resolution. This can be important in making better retrievals of atmospheric quantities.

This correction can also be used to average the 85 GHz channels to match the 37 GHz resolution when uniform spatial resolution is required.

(3-2) Enhancement of SSM/I Images Using Image Reconstruction Techniques: Problem Formulation and SIR Algorithm

In order to develop a method for estimating the brightness temperature on a higher resolution grid $T_B(x,y)$ from antenna temperature measurements $T_A(i)$.

We consider the desired resolution grid with pixel values $T_B(x,y)$ to be estimated and a set of measurements $T_A(i)$ whose bounding rectangles are completely contained within the region of interest (figure 2).

Assuming that the brightness temperature is constant within each pixel:

$$T_A(i) = \frac{1}{\overline{G}_i} \sum_{x=L}^{R} \sum_{y=B}^{T} T_B(x,y) G_i(x,y) \tag{47}$$

where

$$\overline{G}_i = \sum \sum G_i(x,y)$$

and L,R,B,T define a bounding rectangle for the ith measurement.
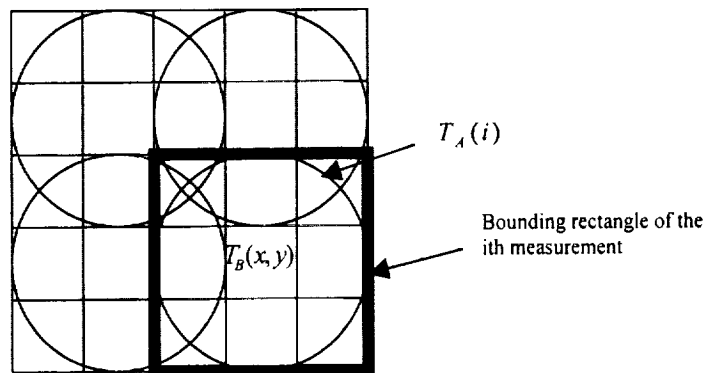

19

Figure 2: bounding rectangles that approximate antenna temperature measurements

Denoting the desired resolution brightness temperature value $T_B(x,y)$ by vector S where S is an N dimensional vector of $T_B(x,y)$ in lexicographic order, the radiometer measurements $T_A(i)$ by vector Z of dimension $M \times 1$ and let H be an $N \times M$ matrix containing the weighting function of corresponding antenna gain function h_{ij}

Where $0 \le h_{ij} \le 1$, which are functions of the antenna gain function and location.

Then we obtain a matrix equation relating the measurements in Z to H and S as:

$$Z = HS + V \qquad (48)$$

Where V is an M dimensional vector of the noise terms v_i, $i = 1, \ldots M$.

Depending on the resolution element size and the number of measurements Z, H can be either over or under determined.

The elements of matrix H are computed by determining the intersection of the measurements and the resolution elements. We can assume that the entries of H are either 1 or 0. The resulting matrix is very sparse though it may be extremely large.

With this formulation, the problem of obtaining estimates of T_B is reduced to the solution of an ill posed linear system of equations which is similar to classic image reconstruction problems in signal and image processing.

5) Scope of Current and Future Work

The AMSR instrument was launched in the year 2000 aboard the Japanese ADEOS-II platform. AMSR observations will be collected in scans of 196 observations over a width of 1600km. The spacing between observations is approximately 10 km for all but the highest frequency and approximately 5 km for the highest frequency. Due to the conical scan geometry, the density of observations increases at the edges of the scan. Table 2 summarizes the range of time integrated AMSR footprint sizes.

The only previous work that has been done to match the resolution of the AMSR measurements was that of Ashcroft and Wentz [16], where they used the BGI method to match the resolution of AMSR channels. Their work didn't not include any enhanced resolution in order to avoid noise amplification. Instead, each set of actual observations is resampled to one of several lower resolutions corresponding to that of 6.9 GHz, 10.7, 18.7, 36.5 GHz and 89 GHz channels.

Ashcroft and Wentz [16], have also addressed the artifacts of the BGI method when used to match the resolutions of AMSR channels. They analyzed the tradeoff between

20

resolution matching and noise amplification for one combination of AMSR channels at one particular point in the scan where they show that because the scan geometry changes across the scan, the precise relationship between smoothing, noise and resolution matching will also vary. This problem appears in choosing the parameter γ which trades off resolution and noise as described in the previous sections.
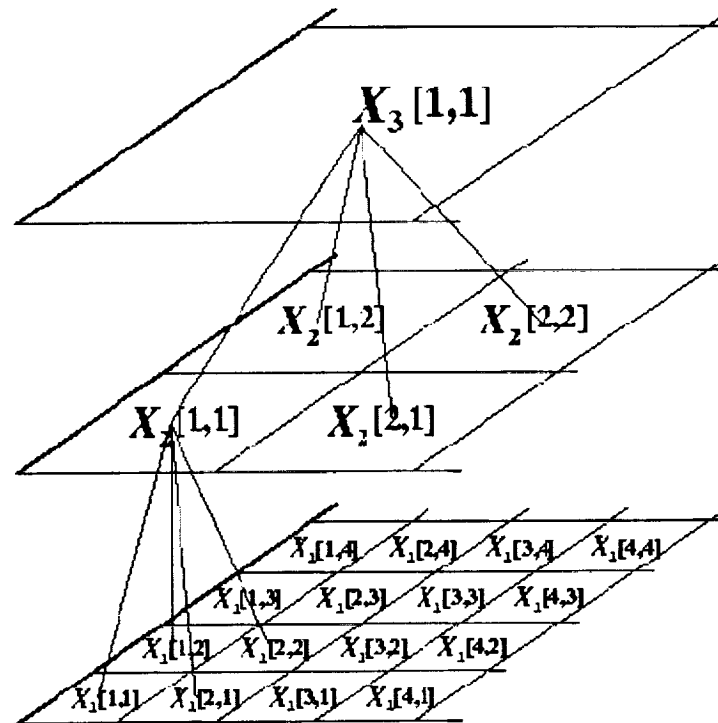
In addition, they addressed the computationally intensive task of calculating the weighting coefficients which is considered as a more challenging problem over the SSM/I case because of the higher density of measurements of the AMSR instruments which means increased number of calculations.

Table 2

Channel Frequency	Resolution (km) along		Sampling interval (km) Along track/scan
	Track	Scan	
6.9	70	40	10
10.7	45	26	10
18.6	27	17	10
23.8	20	13	10
19.35	13.5	43	10
36.5	60	11	10
50.3	9	10.5	10
52.8	9	10.5	10
89	5.3	5.5	5

Motivated by the previous work that has been done for enhancing and matching the resolution of SSM/I measurements, we are going to introduce a new algorithm for enhancing the resolution of AMSR images by utilizing the techniques described in the previous sections taking into account the different nature of the AMSR instrument where the number of frequency channels used is increased over SSM/I channels and the different sizes of the footprints in addition to the spacing between measurements and noise margins introduced by the instrument.

Our new approach uses to advantage the different resolutions from the antenna by constructing a hierarchy of scales which is in turn used to efficiently compute a model relating them. This hierarchical structure as shown in Figure 3, lends itself to not only a parallelization and simple hardware implementation. When resolutions are harmonized across modalities, in a systematic, and reliable way our next objective will be to develop

21

$X_3[1,1]$

$X_2[1,2]$ $X_2[2,2]$

$X_2[1,1]$ $X_2[2,1]$

$X_1[1,4]$ $X_1[2,4]$ $X_1[3,4]$ $X_1[4,4]$

$X_1[1,3]$ $X_1[2,3]$ $X_1[3,3]$ $X_1[4,3]$

$X_1[1,2]$ $X_1[2,2]$ $X_1[3,2]$ $X_1[4,2]$

$X_1[1,1]$ $X_1[2,1]$ $X_1[3,1]$ $X_1[4,1]$

data.

References:

[1] P. Colli Franzone, L. Guerri, B. Taccardi, and C. Viganoti, " Finite element approximation of regularized solutions of inverse potential problem of electrocardiography and application to experimental data," Calcolo, vol. XXII, pp. 91-186,1985.

[2] R. L. Lagendijk and J. Biemond, " iterative identification and restoration of images", Kluwer Academic Publisher, 1991.

[3] *Ku, T.-K.; Kuo, C.-C.J.* , "Design and analysis of Toeplitz preconditioners," Signal Processing, IEEE Transactions on , Volume: 40 Issue: 1 , Jan. 1992 Page(s): 129 –141.

[4] *Chalidabhongse, J.* , "A preconditioning technique for fast iterative image restoration," Circuits and Systems, 1992. ISCAS '92. Proceedings., 1992 IEEE International Symposium on , Volume: 5 , 1992 , Page(s): 2457 -2460 vol.5

[5] Y. Censor, "Finite Series-Expansion reconstruction methods," *proc. IEEE*, vol. 71, pp. 409-419, Mar. 1983.

[6] B. R. Freiden, "Restoring with maximum likelihood and maximum entropy," J. Opt. Soc. Amer., vol. 62, pp 511-518, 1972.

[7], A Ben Hamza and H. Krim, "Towards a unified view of estimation: Vriational vs. Statistical".

[8] A. Strogyn, "Estimates of brightness temperatures from scanning radiometer data," *IEEE Trans. Antennaa and Propagat.*, vol. AP-26, pp. 720-726. 1978.

[9] G. Backus and F. Gilbert, "Uniqueness in the inversion of inaccurate gross earth data," *Phil. Trans. Roy. Soc. London*, vol. A266, pp. 123-192, 1970.

[10] T. T. Willheit, and A.T.C. Chang, "An algorithm for retrieval of ocean surface and atmospheric parameters from the observations of the scanning Multichannel Microwave radiometer(SMMR)", *Radio Science*, vol. 15, pp. 525-544, 1980.

[11] *Poe, G.A.* , "Optimum interpolation of imaging microwave radiometer data," Geoscience and Remote Sensing, IEEE Transactions on , Volume: 28 Issue: 5 , Sept. 1990, Page(s): 800 –810.

[12] *Farrar, M.R.; Smith, E.A.* , "Spatial resolution enhancement of terrestrial features using deconvolved SSM/I microwave brightness temperatures", Geoscience and Remote Sensing, IEEE Transactions on , Volume: 30 Issue: 2 , March 1992 , Page(s): 349 –355

[13] *Robinson, W.D.; Kummerow, C.; Olson, W.S.* , "A technique for enhancing and matching the resolution of microwave measurements from the SSM/I instrument," Geoscience and Remote Sensing, IEEE Transactions on , Volume: 30 Issue: 3 , May 1992 , Page(s): 419 –429.

[14] *Long, D.G.; Daum, D.L.* , "Spatial resolution enhancement of SSM/I data," Geoscience and Remote Sensing, IEEE Transactions on , Volume: 36 Issue: 2 , March 1998 , Page(s): 407 –417

[15] D. S. Early and D. G. Long, " Image reconstruction and enhanced resolution imaging from irregular samples," *IEEE trans. Geoscience and Remote Sensing*, vol. 39, Feb. 2001.

[16] P. Ashcroft and F. J. Wentz, "Resampling of Microwave Radiometer Observations for Spatial Matching," Geoscience and Remote Sensing Symposium Proceedings, 1998.

[17] F. J. Wentz, "Algorithm theoretical basis document, AMSR ocean algorithm," *RSS Tech. Proposal 121599A*, Dec. 15, 1999.

[18] A. Kim, H. Krim, "Hierarchical Stochastic Modeling of SAR Imagery for Segmentation/Compression, " *IEEE Trans. Signal Process.*, vol. 47, No. 2, Feb. 1999.

[19] *Long, D.G.; Hardin, P.J.; Whiting, P.T.* , "Resolution enhancement of spaceborne scatterometer data," Geoscience and Remote Sensing, IEEE Transactions on , Volume: 31 Issue: 3 , May 1993 , Page(s): 700 –715

[20] *Chinn, G.; Sung-Cheng Huang* , "A general class of preconditioners for statistical iterative reconstruction of emission computed tomography," Medical Imaging, IEEE Transactions on , Volume: 16 Issue: 1 , Feb. 1997 Page(s): 1 –10.

[21] P. P. B. Eggermont, G. T. Herman and A. Lent, "iterative algorithms for large partitioned linear systems, with applications to image reconstruction," Linear Alg. Its Appl., vol 40, pp 37-67, 1981